ORIGINAL PAPER

Optimization of Offshore Steel Jackets: Review and Proposal of a New Formulation for Time-Dependent Constraints

Iván Couceiro[1] · José París[1] · Fermín Navarrina[1] · Raquel Guizán[1] · Ignasi Colominas[1]

Abstract

In this work, a methodology for the optimization of offshore wind turbine substructures (jacket type) is presented. The use of a coupled model allows for capturing the full dynamic interaction between all the elements. The structural analysis is carried out in the time-domain. A non-linear integration scheme is necessarily applied due to the effects of the rotation of the blades. Environmental actions, such as wind and waves, are considered as loading conditions. Fatigue damage at the welds of the joints is taken into account. The objective function to be minimized is the weight of the structure. The shape and sizing optimization model is stated in terms of two variables that define the overall shape of the jacket, along with the dimensions of the cross-sections of the structural members. The model is subjected to Ultimate Limit Stress (ULS), Fatigue Limit State and natural frequency constraints. The time-dependent ULS constraints are efficiently treated by means of a new formulation that is based on constraint aggregation. Fatigue accumulation during the whole design life of the structure is accurately assessed, without the need for excessively costly numerical simulations. The optimization problem is solved by means of Sequential Linear Programming, what requires a full first order sensitivity analysis to be performed. The efficiency, reliability and robustness of the proposed methodology is demonstrated by optimizing a real jacket design.

Keywords Structural optimization · Structural dynamics · Offshore jackets · Fatigue

1 Introduction

Wind energy has been one of the main and most successfull strategies over time in the quest for renewable massive power resources . In the last decade, the interest of the industry has turned from the traditional inland concept to the new offshore wind turbine (OWT) farms that are being designed and installed at present. As a general rule, OWTs are meant to increase the efficiency of power extraction by taking advantage of the stronger and steadier wind regimes in open waters, and they can be much bigger than their inland counterparts. Obviously, this severe separation between generation and consumption, along with the inclemency of the enviromental conditions and the difficulty of the installation itself, entails a number of drawbacks and significant engineering challenges. Without any doubt, the first and most restricting factor is the need to build substructures

that could support the wind turbine towers over the sea level in locations where the depth can be as large as the size of the whole system, including the blades, or even greater. There are numerous types and concepts of substructures for this purpose, each of them particularly suitable or only viable for certain ranges of depths, as shown in Fig. 1. While floating type concepts are mostly at the level of drafts and prototypes, bottom supported structures are solidly endorsed by the very wide engineering experience that has been accumulated over time by the offshore oil and gas industry [1].

The current critical challenge in this technology is the deployment of OWT in intermediate water depths, from 30 to 60 m, where the jacket type structures have already proved their efficiency. Nevertheless, a number of features in the jacket analysis and design are still subject to uncertainties, or simply unresolved. The mere structural analysis of the jackets and the definition and fulfillment of the particular strength requirements is a cumbersome process. Some of the physical phenomena that are critical to the design life of the structure, are hard to assess with accuracy. And the correct modelization of the in-place environmental conditions may require the definition of an important number of

✉ Iván Couceiro
  ivan.couceiro.aguiar@udc.es

[1] Group of Numerical Methods in Engineering, Universidade da Coruña, Campus de Elviña, 15071 A Coruña, Spain
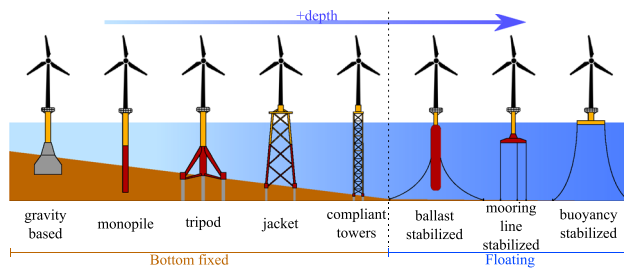
Fig. 1 Offshore substructures concepts for increasing water depth

load cases that generate an even greater amount of structural output results, running over the capacity of data processing and storage. These characteristics make the design of steel jackets a hard task itself, what hinders the application of optimization techniques to this kind of problems.

A fully-coupled model for the optimization of jacket substructures considering the dynamic response and fatigue damage is presented in this paper. A novel formulation to deal with time-dependent constraints from structural dynamic problems is introduced and long-term fatigue damage is assessed using short-time numerical simulations.

The outline of the paper is as follows. First, a state of the art review of the optimization of offshore jackets is presented in Sect. 2, then the structural model is presented in Sect. 3. The loading conditions for the in-place structure are derived from the environmental conditions in Sect. 4. Next, the numerical integration method for solving the dynamic equation of motion is presented in Sect. 5. The optimization problem and the numerical algorithm are exposed in Sects. 6 and 7. Some numerical results are presented to show the robustness of the proposed optimization methodology in Sect. 8. Finally, some conclusions about the exposed formulation and results are drawn.

2 State of the Art on the Optimization of Offshore Jackets

Jacket type substructures as supports for offshore turbines are a relatively new field of interest in comparison with the general bottom-fixed structures traditionally used in the oil and gas industry. The first offshore wind farm that used jackets was the Beatrice Demonstration in 2007. Thus, all the advances in the analysis and design of offshore jackets are reduced to the last decade.

One of the first noteworthy works addressing the structural optimization of wind systems is [2]. Even though it is focused on an onshore turbine case, the optimization of the turbine tower is performed in the time domain considering extreme and fatigue constraints. In [3], a reliability-based optimization is proposed to account for uncertainties in the

design of the jackets. The probabilistic constraints are based in extreme conditions but the formulation can be extended to take into account fatigue accumulation under a probabilistic point of view. In [4] the optimization of a jacket for a platform under extreme loading is presented. The dimensions of the deck and the cross-sections of the main piles of the jacket are considered as design variables, and the process is performed by means of the ANSYS analysis and optimization toolbox. The dimensions of the deck and the cross-sections of the main piles of the jacket are considered as design variables. In [5], the superposition approaches, partially integrated and fully integrated models are compared using Damage Equivalent Loads (DEL) in terms of design optimization. In [6], a jacket for a platform is optimized under extreme loading by means of a genetic algorithm. The diameters and the thicknesses of the tubular members are the design variables, while the weight of the jacket is the objective function to be minimized. Directional environmental data is used for the load cases.

The Norwegian University of Science and Technology has been particularly active in this field in the past years. This progress is reflected in many scientific publications in journals and conferences [7–12]. A common feature of these works is the optimization of the cross-sections of the structural members of the jacket and the utilization of the FEDEM software for the dynamic analysis and load calculations. The use of the Rainflow counting algorithm is also extended in all these works.

In [7] the use of a full-height lattice tower substituting the typical tubular tower is studied. The improvement of the designs is made by locally modifying the dimensions of the elements. Modifications are based on which one is the farthest from its behavioral limit. In [8] a comparison between 3-legged and 4-legged jackets is carried out with an optimization of the 3-legged version. DELs are used and the stability of the members is incorporated as a check out in the optimization loop. Later on this work was extended, including a gradient based optimization with analytical sensitivities of the constraints and the use of Sequential Quadratic Programming (SQP) method of MATLAB [12]. The time-dependent constraints are treated by means of the worst-case approach. In [10] the dynamic analysis is based in 30 s simulations using a genetic algorithm for the optimization and also for analysis shortcuts. In subsequent works a local optimization approach is proposed, assuming that changes in the properties of the members do not significantly affect the response of the structure [11].

It is also worth mentioning the work developed in [13]. Analytical gradients are used for the optimization and a quasi-static structural analysis is performed to evaluate the behavior of the structure. The optimization is carried out by means of the Sequential Linear Programming (SLP) method implemented in the CPLEX optimizer of ILOG-IBM. This is

one of the most complete works in optimization of offshore jacket structures so far, along with [12].

In [14] authors propose a methodology for the integrated optimal design of jackets including the pile foundations including the soil-structure interaction. The combined mass of the jacket and the foundation is minimized under the hypothesis of static analysis and by using a gradient-based numerical optimization method.

3 Structural Model of Coupled Offshore Wind Turbines

Most works base their analysis and optimization process on decoupled models where the target structure, i.e. the jacket, is separated from the turbine. However, it is proved that displacements, stresses and the computed fatigue damage obtained by means of decoupled models may exhibit a significan lack of accuracy with respect to the results delivered by coupled models [15]. A particular advantage of coupled models is the direct consideration of aerodynamic damping [16] without the need for artificial damping ratios or coefficients. Additionally, the management of the dynamic response in terms of an optimization problem is hard to handle both, accurately and efficiently [17].

The proposed model for the optimization of the jacket substructure is a coupled model. Therefore, the computational model includes all the elemens of the complete OWT: jacket, transition piece, turbine tower, blades and rotor-nacelle assembly, as shown in Fig. 2. The usual approach in offshore engineering is to separate the aerodynamic part (tower, rotor-nacelle and blades) and the substructure (jacket) in two different models [18, 19]. Loads are traditionally extracted from the aerodynamic part by using multibody dynamics and then applied separately at the top of the jacket. These models are called decoupled or uncoupled. While they clearly simplify the analysis procedure for the substructure, their main drawback is that it is impossible to capture the dynamic interaction between the aerodynamic part and the jacket. Another phenomenon that can not be simulated either is the aerodynamic damping [16]. Artificial damping ratios need to be introduced in order to account for the reduction in displacements experienced.

The presented fully-coupled model allows to reproduce the dynamic and structural relationship between every element of the OWT. Additionally, the continuous rotation of the blades can be considered in the model in order to analyze its impact on the structural response. However, the rotation is not included as free movement released at the joint of the rotor as produced by the wind exerted torque, but a change of the geometry imposed between time-steps. The latter has a direct impact on how the dynamic equation has to be solved. This is discussed in Sect. 5.

The OWT is modeled as a 3D framed structure with linear beam elements. While each tubular bar between tow joints of the jacket is considered as a single beam element, the tower
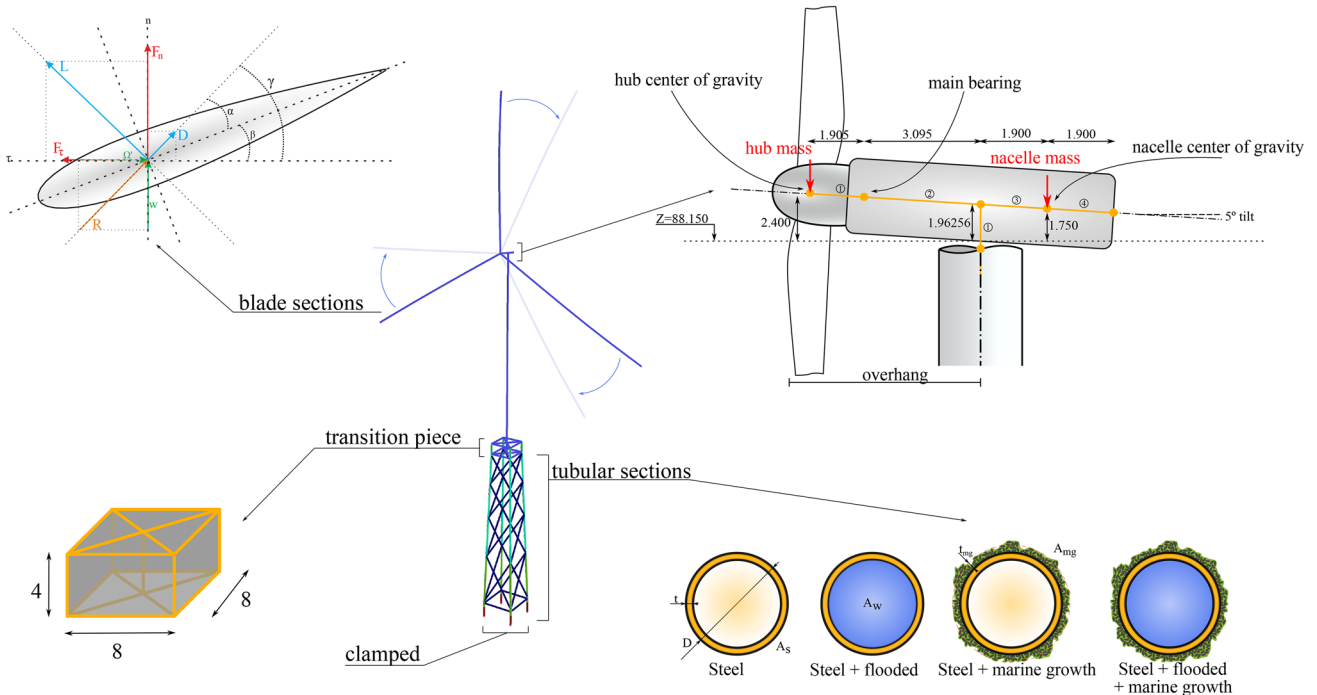

Fig. 2 Schematics of the OWT coupled model

and the blades of the turbine are discretized in a set of elements with the averaged mechanical and aerodynamic properties. Each blade is formed by 50 different elements. The tower is modeled with 8. The clearly non-beam-type structures: transition piece and nacelle, are modeled also by using beam elements which artificial mechanical properties match the mass and stiffness of the real components (see Fig. 2). The system is considered clamped at the bottom.

Therefore, the OWT is structurally and dynamically defined by its global mass, damping and stiffness matrices, M, C and K respectively. Classical damping or Rayleigh damping is considered in terms of the first two natural modes of vibration and damping ratios, as recommended [20, 21]. But, the inclusion of the rotating blades introduces some considerations over the definition of the structural matrices. First, the local reference frame of the rotating sections of the blades have to be defined so that the local z axis remains in the global YZ plane along the rotation. Thus, the orientation of the principal axes of the cross-section is maintained. And second, since the structural matrices are dependent on the geometry of the structure, the imposed rotation generates geometry changes that make those matrices different for every time-step. Thus, at each time-step of the time-integration algorithm M, C and K have to be recalculated, or at least the contributions of the rotating elements. On the other hand, other effects generated by the rotation of the blades, such as centrifugal stiffening and Gyroscopic effect, are neglected.

4 Environmental Model and Loading Conditions

Offshore structures are subjected to a wide range of different types of loads. For example, motions in transport, lifting, launching and other operations generate loads that differ from the in-place loads. Nevertheless, in this work only in-place loading conditions are considered since they constitute the main actions that determine the design of the structure.

4.1 Self Weight and Buoyancy

All the elements of the OWT are subjected to their self weight. The model is also able to take into account the possibility of concentrated masses at certain nodes of the structure. This is of use at the stiffeners of the tower and to model the local mass of the hub. Only translation degrees of freedom are affected by concentrated masses. Additionally, the submerged elements of the jacket experience buoyancy forces. Self weight and buoyancy of the members are computed by using the so called marine method, where the buoyancy force simply reduces the total weight of the element as:

$$W_e = g L \left(\rho_s A_s + \rho_{mg} A_m g + \rho_w A_w - \rho_w A_t \right) \tag{1}$$

where L, ρ and A are length, density and area and subscripts s, mg, w and t refer to steel, marine growth, water, and total area. Conditions for the tubular elements of the jacket are schematically shown in Fig. 2.

Although buoyancy may seem negligible, structural tubular members for offshore structures are often carefully selected such that their buoyancy/weight ratio is close or even greater than 1.0. Thus, the total buoyancy load may be of the order of magnitude of the total weight of the jacket.

4.2 Wind

Wind is the main load acting on the non-submerged part of the structure: the wind turbine tower and the blades. In decoupled models these parts are detached from the substructure, while wind loads are computed by means of suitable specific software and then applied as a time-history of loads at the top of the jacket. On the contrary, the presented coupled model computes the actual loads generated by wind at each time-step and forces are applied at the points where they are actually generated.

The aerodynamic forces on the discrete sections of the blades are computed in the reference frame of the airfoil sections as:

$$\begin{aligned} D &= \frac{1}{2} \rho R^2 C_d c \, \delta r \\ L &= \frac{1}{2} \rho R^2 C_l c \, \delta r \end{aligned} \tag{2}$$

where D and L are the drag and lift forces respectively, ρ is the density of the air, c is the chord length and δr is the length of the discretized element. R is the resultant of the flow direction, considering the velocity of the wind U_d and the rotational speed of the turbine Ω.

Drag and lift coefficients, C_d and C_l, depend on the aerodynamic characteristics of the blade section and the angle of attack of the resultant R. To compute the angle of attack, the Blade Element Momentum theory (BEM) is used. The basics of the method can be consulted in [16, 22, 23]. By means of the BEM theory, the wind speed and effective rotational speed can be computed as:

$$\left. \begin{aligned} U_d &= U_\infty (1 - a) \\ \Omega' &= \Omega r (1 + a') \end{aligned} \right\} \rightarrow R = \sqrt{U_d^2 + \Omega'^2} \tag{3}$$

$$\sin(\gamma) = \frac{U_\infty (1 - a)}{R} \longrightarrow \alpha = \gamma - \beta \tag{4}$$

where U_∞ is the incoming wind velocity at the far upstream and a and a' are the so-called axial and tangential induction

factors that represent the loss in speed at the actuator disc. The angle β is the pitch angle and α is the angle of attack of the inflow direction with respect to the chord-wise axis.

The induction factors are unknowns in Eq. (3) that must be computed by means of an iterative process [16]. Other effects, as the Prandtl's blade tip loss, are considered in the model.

However, the actual forces experienced by the blades are in fact reduced due to the aerodynamic damping phenomenon. Although, torsional deformations may directly influence the angle of attack and therefore modify the resultant drag and lift forces [24], the effect produced by the displacement velocity is more relevant. Figure 3 shows the motion of the blade from the initial position to the deformed position produced by the wind loads. The speed of the movement $\dot{u}$ reduces the apparent wind speed experienced when the blade moves downwind and augments it when it moves upwind. As a result, the real thrust or normal force exerted to the blade is smaller in the downwind movement and higher in the upwind movement. In both cases, the thrust variation ΔT works against the movement of the blade, thus producing a reduction of the actual movement experienced by the structure. That source of structural damping is called aerodynamic damping. While decoupled models are not able to account for it directly, the aerodynamic damping can be easily implemented in the proposed coupled model since displacements and wind loads are computed by the same code at each time-step.

Another effect that significantly reduces the wind loads over the blades is the tower dam effect. Whenever a blade passes in front of the tower it experiences a reduction in the effective wind speed it receives. According to [25] the modified wind speed can be computed as:

$$U_d' = U_d \left(1 - \frac{D_t}{2\pi} \frac{\delta_x}{\delta_x^2 + \delta_y^2} \right) \tag{5}$$
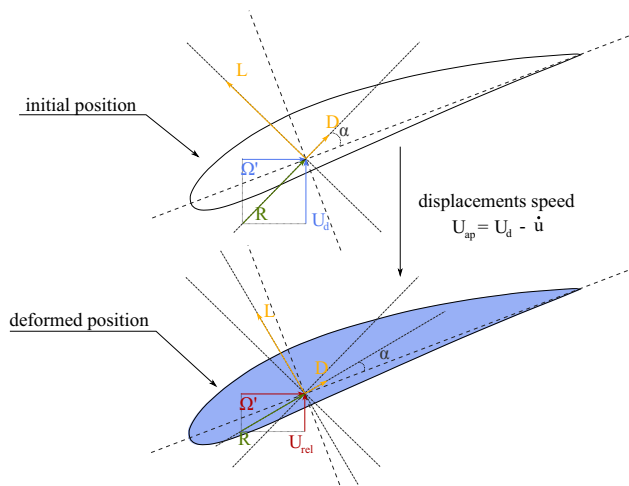

Fig. 3 Aerodynamic damping

being D_t the diameter of the tower and δ_x and δ_y distances between the passing blade and the tower in the global reference frame.

The wind force over the tower of the turbine is computed as:

$$F_t = \frac{1}{2} \rho \, U(h)^2 \, C_d \, D_t \, \delta l \tag{6}$$

where $U(h)$ is the wind speed at elevation h, δl is the length of the element and C_d the drag factor o the cylindrical section. A logarithmic profile of the wind $U(h)$ is used.

4.3 Waves

Waves are the main loads acting on the submerged part of the OWT, which is the jacket substructure. Deterministic theories are the easiest way of describing regular waves. In regular waves properties are invariant from cycle to cycle and are dominated by three parameters: Period T, height H and water depth d. A number of regular wave theories have been developed. Two classical theories, the linear Airy and the Second Order Stokes are usually applied and show good predictions in practice [1]. The 5th order or stream function theory is also widely used.

Kinematic properties can be obtained from analytic expressions of the regular waves. The kinematic properties are the velocity and acceleration of particles in the direction of propagation and in the vertical direction. For slender members it is accepted that wave loads can be assessed by using Morison's formula [26]. Then, the normal force per unit of length exerted by the fluid flow in a direction perpendicular to the element is:

$$\begin{aligned} f_N(x, z, t) &= \frac{\pi}{4} \, \rho_w \, C_M \, D^2 \, \dot{s}(x, z, t) \\ &+ \frac{1}{2} \, \rho_w \, C_D \, D \, s(x, z, t) |s(x, z, t)| \end{aligned} \tag{7}$$

where the force is decomposed into two sources: an inertial force that depends on the inertia coefficient C_M, the diameter of the element D and the acceleration of the fluid $\dot{s}$; and a drag force that is proportional to the drag coefficient C_D, the diameter of the element and the velocity of the fluid particles s.

Equation (7) can be also used to account for ocean current by adding the current velocity to the speed of the waves. When dealing with compliant structures the effect of the movements in the structure can additionally be incorporated in terms of relative velocities and accelerations.

4.4 Environmental Data and Load Cases

Particular load cases under normal conditions for OWT include wind and wave specific situations which are normally related between them. For short-term simulations it is

common to use power spectrum functions to determine the wave conditions. However, wave and wind conditions for the long-term simulations can again be modeled using generic distributions or in terms of a scatter diagram. Scatter diagrams provide the occurrence of a given state. For example, the frequency at which a given (H, T) pair appears for wave loading. There are directional scatter diagrams that account for the direction of both wind and waves.

In order to represent correctly the actual conditions that the OWT will bear, most combinations from the scatter diagram must be included, or at least those sea states with a relevant probability of appearance. However, each sea state combination of wave height and period is also associated with a particular wind speed. Since different wind speeds produce different rotational speeds of the turbines, the rate of change of the structural properties of the OWT, measured by the change in matrices M, C and K, will be different for each load case. Therefore, as stated in section 3, the structural matrices in the time history analysis will be different not only for each time-step, but also for each design load case.

The latter implies a severe amount of information to be stored and processed at each step of the time integration scheme. Added to the huge amount of output data needed to assess the fatigue damage (5), current models are highly limited in terms of the number of actual load cases that can be considered for a simple structural analysis. Obviously, the cost increases heavily if an optimization process is performed.

5 Dynamic Analysis and Fatigue Damage Assessment

To capture the dynamic response (in displacements and stresses) of the structural elements, the discrete equation of motion has to be solved:

$$M\ddot{u} + C\dot{u} + Ku = f \tag{8}$$

where u, $\dot{u}$ and $\ddot{u}$ are the global displacements, velocities and accelerations of the degrees of freedom of the structure and f are the time-dependent external forces.

Previous to solving Eq. (8), the structural system must be dynamically characterized through the natural frequencies and modes of vibration (see Fig. 4). These natural frequencies will be of importance in section 6 for defining the optimization problem. They are also needed for assembling the Rayleigh damping matrix C as a combination of the mass matrix M and the stiffness matrix K.

5.1 Time Integration Scheme

As it was stated, the environmental data and the rotation of the blades led to a high computational effort. Moreover, applicable standards such as [28] state that the dynamic response of the structure must be evaluated during a sufficiently large period of time (at least 10 min) which is also the averaging time for short-term wind conditions. Running such simulations call for a large enough time-step in order to compute a reasonable number of integration steps while keeping the required accuracy. Thus, an efficient and low resource-demanding integration algorithm is indispensable.

One of the most extended direct integration methods is the Newmark family methods [29]. The parameters of the method can be adjusted so the integration scheme is unconditionally stable for any size of the time-step. However, the definition of our dynamic problem, and in particular the large changes in geometry caused by the rotation of the blades, requires the utilization of a non-linear time integration scheme. Newton iterations can be added at each time-step of the Average Acceleration method (a method of the Newmark family) to adapt it to non-linear systems.
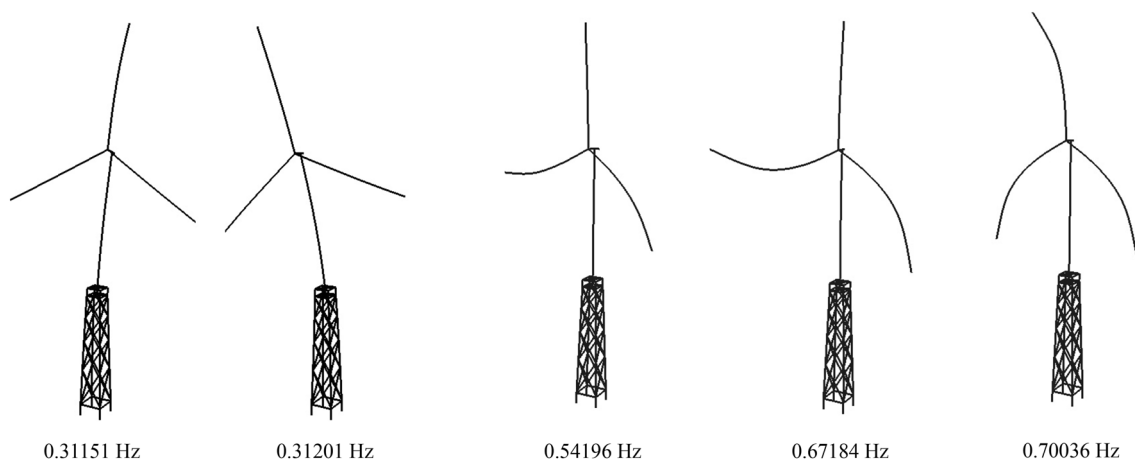

| 0.31151 Hz | 0.31201 Hz | 0.54196 Hz | 0.67184 Hz | 0.70036 Hz |

Fig. 4 First natural frequencies and modes of vibration obtained with the proposed model for the OWT of [27]

The solution of the variable geometry problem with the non-linear algorithm and the update at each time step of the finite element matrices yields an increase in the needed computing effort. In practice the computational time needed for the simulation is triplicated. That proportionality is maintained with Δt. In Fig. 5 a model with 1428 degrees of freedom is shown.

In fact, the Average Acceleration method looses its unconditional stability property in its non-linear version [30]. The main problem is that it is a step by step integration method, and the changes in the structure are updated only at the beginning of each step. The linearization of the structural changes between time-steps may lead to poor accuracy and instability. Thus, the time-step must be limited in order to guarantee the stability of the integration method.

5.2 Fatigue Damage

One of the most challenging problems in offshore steel structures is the assessment of fatigue. The inherent cyclic nature of wind and wave loading makes the steel jackets particularly susceptible to experiment fatigue damage. This effect is specially critical at the locations where there is an exceptional concentration of stresses, as it happens at the welds between the tubular elements of the jacket.

There are two main theories to calculate fatigue damage. The first is fracture mechanics and the second involves methods to account for the accumulated damage of the cyclic loading. The latter is the extended method recommended by offshore standards.

In particular, the Stress-Cycle (S-N) approach is the one used. The S-N curves (or Wöhler curves) represent the number of cycles N of a given constant stress range S that can cause failure of the structure by fatigue. S-N curves are fully documented [31] and are based upon extensive collections of experimental data.
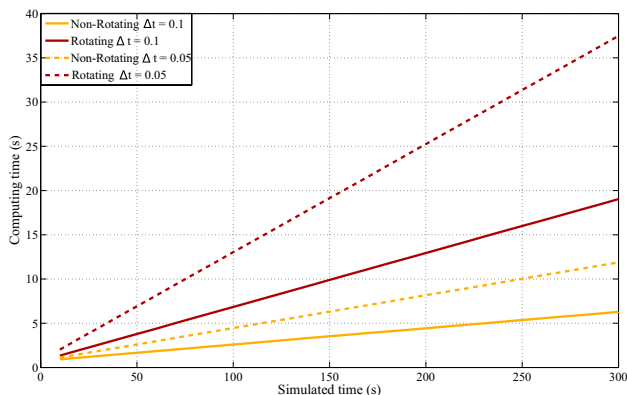

Fig. 5 Rotating vs non-rotating computing time for the time integration using the Newmark and the non-linear Newmark algorithm

Some additional hypothesis are taken. First, it is assumed that each stress range produces a linear damage based only on the number of appearances. Thus, for a given stress range $\Delta\sigma_i$ the damage produced D_i would be:

$$D_i = \frac{n_i}{N_i} \tag{9}$$

where n_i is the number of stress cycles with amplitude $\Delta\sigma_i$ that appear in the structure and N_i is the number of cycles to failure for that stress range given by the S-N curve.

Second, it is assumed that damages associated with different stress ranges are completely independent from each other, meaning that the time and the sequence in which the stress cycles take place are irrelevant. This hypothesis and methodology to compute the damage is known as the Palmgren-Miner rule [32]. Since the number of cycles to failure N_i are given by the S-N curves as a function of the stress-cycles amplitude $\Delta\sigma_i$ as $N_i = \dfrac{\overline{a}}{(\Delta\sigma_i)^m}$, the total damage can be computed:

$$D = \sum_{i=1}^{k} \frac{n_i}{N_i} = \frac{1}{a} \sum_{i=1}^{k} n_i (\Delta\sigma_i)^m \tag{10}$$

where $\overline{a}$ and m are parameters of the S-N curve and k is the number of different amplitude stress-cycles that appear.

There are different S-N curves for different geometries and environmental conditions. The curve for tubular joints in seawater with cathodic protection (which is the adequate for the offshore jackets) leads to:

$$D = \frac{1}{a} \sum_{i=1}^{k} n_i \left(\frac{t}{t_r}\right)^{k'm} (\Delta\sigma_i)^m \tag{11}$$

where t is the thickness of the tubular element and t_r is a reference thickness (32 mm). k' is a thickness exponent taken as 0.1 for tubular welds. The term $\left(\dfrac{t}{t_r}\right)^{k'}$ is added to extend the S-N curves to any cross-section.

5.3 Hot-Spot Stresses and Stress Concentration Factors

As mentioned before, the welds of the joints are the points susceptible of fatigue failure. At these points, the nominal stresses can be obtained by means of the proposed beam formulation. However, they have to be scaled by the so-called Stress Concentration Factors (SCF). These SCF are introduced to account for the exceptional stress peaks that appear at the joints. The values of the SCF depend exclusively on geometrical parameters. Factors used in this work correspond to those defined in the standards [31]. The SCF equations were obtained by experiments in [33]. Each joint is also considered to have eight

hot-spots uniformly distributed at the circumference of the intersection where fatigue must be evaluated as seen in Fig. 6.

The hot-spot stress at each joint is then calculated as:

$$\sigma_1 = (\text{SCF}_{\text{AC}})\,\sigma_x + (\text{SCF}_{\text{MIP}})\,\sigma_{my} \tag{12}$$

$$\sigma_2 = \frac{1}{2}(\text{SCF}_{\text{AC}} + \text{SCF}_{\text{AS}})\sigma_x + \frac{1}{2}\sqrt{2}(\text{SCF}_{\text{MIP}})\sigma_m y \\ - \frac{1}{2}\sqrt{2}(\text{SCF}_{\text{MOP}})\sigma_m z \tag{13}$$

$$\sigma_3 = (\text{SCF}_{\text{AS}})\,\sigma_x - (\text{SCF}_{\text{MOP}})\,\sigma_{mz} \tag{14}$$

$$\sigma_4 = \frac{1}{2}(\text{SCF}_{\text{AC}} + \text{SCF}_{\text{AS}})\sigma_x - \frac{1}{2}\sqrt{2}(\text{SCF}_{\text{MIP}})\sigma_m y \\ - \frac{1}{2}\sqrt{2}(\text{SCF}_{\text{MOP}})\sigma_m z \tag{15}$$

$$\sigma_5 = (\text{SCF}_{\text{AC}})\,\sigma_x - (\text{SCF}_{\text{MIP}})\,\sigma_{my} \tag{16}$$

$$\sigma_6 = \frac{1}{2}(\text{SCF}_{\text{AC}} + \text{SCF}_{\text{AS}})\sigma_x - \frac{1}{2}\sqrt{2}(\text{SCF}_{\text{MIP}})\sigma_m y \\ + \frac{1}{2}\sqrt{2}(\text{SCF}_{\text{MOP}})\sigma_m z \tag{17}$$

$$\sigma_7 = (\text{SCF}_{\text{AS}})\,\sigma_x + (\text{SCF}_{\text{MOP}})\,\sigma_{mz} \tag{18}$$

$$\sigma_8 = \frac{1}{2}(\text{SCF}_{\text{AC}} + \text{SCF}_{\text{AS}})\sigma_x + \frac{1}{2}\sqrt{2}(\text{SCF}_{\text{MIP}})\sigma_m y \\ + \frac{1}{2}\sqrt{2}(\text{SCF}_{\text{MOP}})\sigma_m z \tag{19}$$
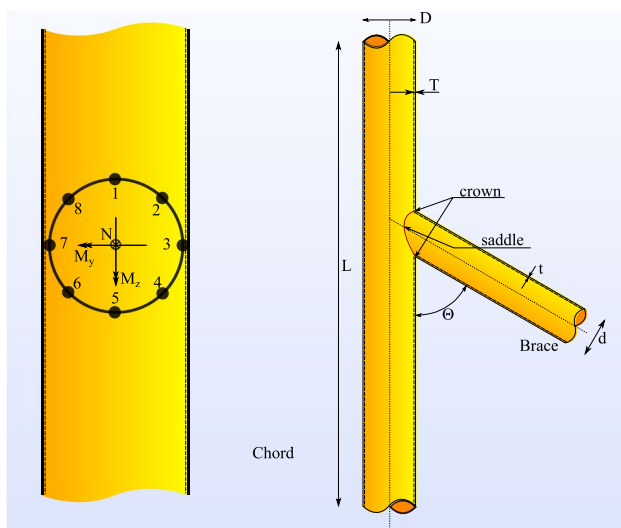
Fig. 6 Geometrical definition for tubular joints (T/Y joint)

where σ_x, σ_{my} and σ_{mz} are the nominal stresses due to axial forces and moments. SCF_{AC} and SCF_{AS} are the SCF corresponding to axial loading at the crown and the saddle. SCF_{MIP} and SCF_{MOP} are the SCF for the in-plane and out-of-plane bending moments respectively.

5.4 Stress Cycles Counting Process

The carried out dynamic structural analysis produces a random-shaped peaks distribution of stresses which complicates the determination of the number of stress-cycles that appear. Special counting algorithms must be used in order to extract the number of cycles at each range of stress . There are numerous counting algorithms and methods but, among the most used ones, the Rainflow counting method [34] is the recommended method in fatigue analysis.

The procedure was intentionally developed to count the cycles of strain in metals to account for fatigue. In fact, it is the method adopted by the American Society for Testing Materials (ASTM) [35]. The standard comprises a set of rules to extract the cycles and half-cycles from time-history of stresses.

5.5 Long-Term Fatigue Damage Assessment

Even though there is a method to count the number of stress cycles that the elements of the jacket experiment, it is completely unpractical to count every single cycle during the whole design life of the structure and for all the possible load scenarios. Thereby it is mandatory to develop techniques to estimate the long-term damage from shorter calculations.

Most techniques for damage estimation are based on two strategies. The first is based on very short time simulations or even on simulating singular events (for example one single wave). The second group of methods are based on adjusting probability functions of the stress-cycles. However, neither the short time series were capable of assessing the damage for the long-term nor the long computations were manageable or the probabilities obtained were representative enough. One of the alternatives is to estimate the fatigue damage by using spectral methods. In this regard, the Probability Density Function (PDF) of the stress ranges can be estimated by using the Dirlik's method [36]. However, a well-known limitation of this method is that it is unable to capture any bimodal character of a stress signal and fails to model signals with large periodicity which often appear in wind turbines [37]. Moreover, since the Dirlik's method is based on the power spectrum, it contains information on the amplitudes but not on the phases, so it can not account for two or more signals that are in phase, thus producing a higher estimated damage. Spectral and frequency domain analysis allow for an easier handle of the problem. However,

these methods show lower accuracy when compared with time-history methods [38].

Thus, the common trend in offshore engineering and particularly in the assessment of fatigue for wind turbines is the time history analysis [19, 39, 40]. For example, in [41] the estimation of fatigue from a linear regression based on Damage Equivalent Loads (DEL) for 10 min time-series is studied with promising results. Other authors have performed a topology optimization of a jacket using 30 s-long simulations, considering that the cycles found in that interval were repeated a number of times (design life/simulation time) [42].

Given the assumptions implied in the Palmgren-Miner rule, it is reasonable to think that the damage will continue to increase linearly. In this work a linear extrapolation model is presented for the estimation of long-term fatigue damage from shorter simulations.

For the short-term simulations, significant enough data is needed so that the loads and the structural response are completely developed. It is also necessary to make sure that high period cycles are not being cut out. The computational cost of the method must remain manageable. Since offshore standards recommend the 10 min period for the loading simulations, the linear extrapolation proposed in this work is based on the damage computed for 300 and 600 s. Note that the extrapolation is performed in the damage values and not in the number of cycles. For a given design life T_L in seconds, the expected damage is stated as:

$$D_L = D_{300} + \frac{D_{600} - D_{300}}{300}\left(T_L - 300\right) \tag{20}$$

Figures 7 and 8 show two examples of the linearly estimated damage for a reference jacket. In both figures the points represent the damage obtained with simulations of the whole time-interval: 300, 600, 3600, 86,400 and 630,720,000 s. The dashed lines draw the estimated damage calculated using Eq. (20).

6 Optimization Problem and Time-Dependent Constraint Handling

The final objective of this work is to develop a numerical technique for the optimization of jackets for OWT, considering the dynamic interaction between elements in a fully-coupled model and the fatigue damage. This section is intended to deal with the definition of the optimization problem and the treatment of the time-dependent constraints.

The standard optimization problem can be written as:

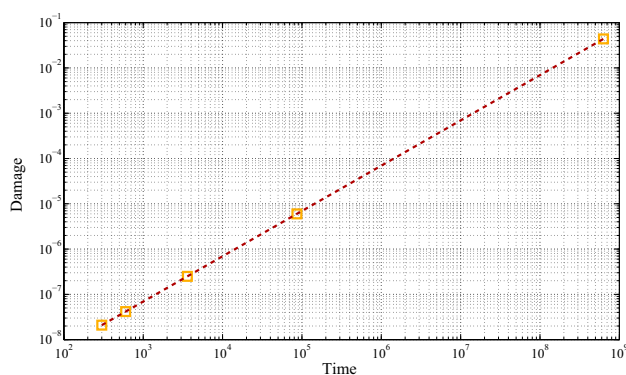$$\min F(\boldsymbol{x}) \tag{21}$$

subject to:

Fig. 7 Calculated vs estimated damage for bar 121, node 2 hot-spot 1 of a reference model
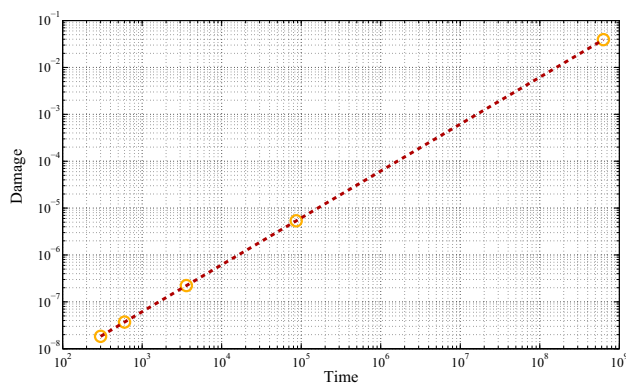

Fig. 8 Calculated vs estimated damage for bar 33, node 1 hot-spot 2 of a reference model

$$\begin{aligned} g_j(\boldsymbol{x}) \leq 0; & \quad j = 1, m \\ h_k(\boldsymbol{x}) = 0; & \quad k = 1, l \\ x_i^m \leq x_i \leq x_i^M; & \quad i = 1, n \end{aligned} \tag{22}$$

where F is the objective function that depends on the set of n design variables $\boldsymbol{x}$, g_j are the m inequality constraints, h_k are the l equality constraints and x_i^m and x_i^M are the minimum and maximum value of the design variables, the side constraints. In the following sections, the optimization problem, symbolically represented by 21 and 22, is described in detail. All the constraints are expressed as inequality constraints.

6.1 Objective Function and Design Variables

The structural optimization of the jacket is defined as a weight minimization problem. Considering the individual weight of the discrete elements of the jacket, the objective function is:

$$F = \rho_s \sum_{i=1}^{n} \left(\frac{\pi}{4} \left(D_i^2 - (D_i - 2t_i)^2 \right) \right) l_i \qquad (23)$$

where ρ_s is the steel density, D_i, t_i and l_i are the diameter, thickness and length of the i-th element and n is the number of elements of the jacket.

A sizing optimization problem is proposed using the dimensions of the tubular elements D_i and t_i as design variables and the width of the bottom and the top of the jacket μ_B and μ_T, allowing the general outline of the structure to vary, as seen in Fig. 9.

6.2 Design Constraints

The set of structural constraints imposed to the optimization problem is based on the requirements specified by the applicable standards [20, 43].

The optimization problem is formulated using the following constraints: Fatigue Limit State (FLS) constraints set a limit for the fatigue damage at the joints of the structure. Natural frequency constraints impose restrictions to the first natural modes of vibration of the structure. Finally, Ultimate Limit State (ULS) constraints limit the stress level over the tubular elements at every instant of the dynamic problem.

6.2.1 Fatigue Limit Stress Constraints

The Fatigue Limit Stress constraint (FLS) ensures the feasibility of the jacket during its design life under normal state operational conditions. In order to consider all the possible environmental conditions, each load case is weighted by a probability of appearance. Also, the fatigue damage is limited by a usage factor called Design Fatigue Factor (DFF). DFF can take values up to 10. In most cases (for example for hot-spots located in non-accessible areas and not planned for inspection or repair) a value of 3 is advised. Thus
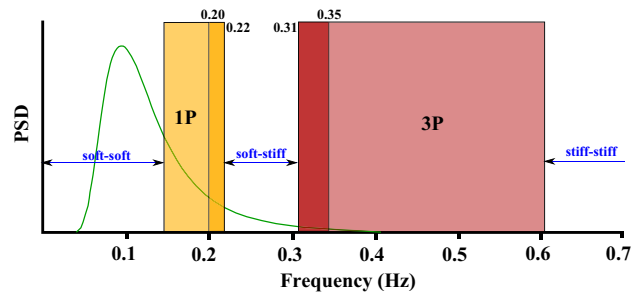

Fig. 9 Design variables for the optimization problem

Fig. 10 1P and 2P frequency bands for the natural frequency constraints

$$g_F = \sum_{l=1}^{N_p} P_l \frac{1}{a} \sum_{i=1}^{k} n_i \left(\frac{t}{t_r} \right)^{k'm} \left(\Delta\sigma_i \right)^m - \frac{1}{\text{DFF}} \leq 0 \qquad (24)$$

where N_p is the total number of considered load cases and P_l is the probability of appearance of each load case.

The SCF parameters defined in [31] have been validated under certain geometrical limitations of the geometry of the joints. Thereby a group of geometrical constraints have to be included to guarantee the validity of the used SCF:

$$\left\{ \begin{array}{l} g_{\beta m} = 0.2 - \dfrac{d}{D} \leq 0 \\[2mm] g_{\beta M} = \dfrac{d}{D} - 1.0 \leq 0 \end{array} \right\} \left\{ \begin{array}{l} g_{\tau m} = 0.2 - \dfrac{t}{T} \leq 0 \\[2mm] g_{\tau M} = \dfrac{t}{T} - 1.0 \leq 0 \end{array} \right\} \qquad (25)$$

$$\left\{ \begin{array}{l} g_{\gamma m} = \dfrac{1}{4} - \dfrac{D}{64T} \leq 0 \\[2mm] g_{\gamma M} = \dfrac{D}{64T} - 1.0 \leq 0 \end{array} \right\} \left\{ \begin{array}{l} g_{\alpha m} = \dfrac{1}{10} - \dfrac{L}{20D} \leq 0 \\[2mm] g_{\alpha M} = \dfrac{L}{20D} - 1.0 \leq 0 \end{array} \right\} \qquad (26)$$

$$\left\{ \begin{array}{l} g_{\theta m} = \dfrac{4}{9} - \dfrac{4\theta}{\pi} \leq 0 \\[2mm] g_{\theta M} = \dfrac{4\theta}{\pi} - 1.0 \leq 0 \end{array} \right\} \qquad (27)$$

where the dimensions are those depicted in Fig. 6.

6.2.2 Natural Frequency Constraints

Offshore wind turbines are particularly dynamic sensitive due to the multiple cyclic loading and forcing frequencies. There are two forcing frequencies, the first is the rotational frequency of the rotor, usually called 1P. In addition, to tower dam effect generates another excitation frequency called the blade-passing frequency, usually denoted by 3P.

Figure 10 draws those two bands and the three available design domains: soft-soft, soft-stiff and stiff-stiff. Designs
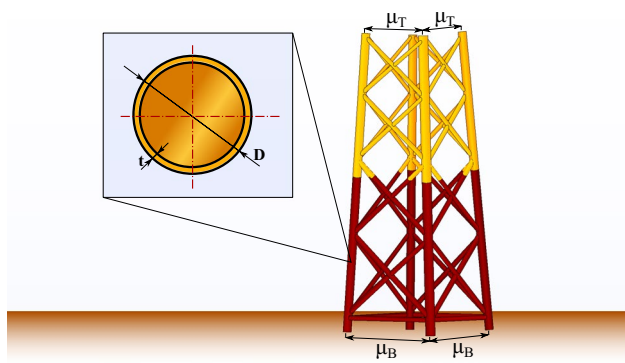
of jackets are recommended to fall in the soft-stiff region. The soft-soft domain is avoided since it is close to the typical peak frequency of the waves and the stiff-stiff region is rejected because it generates over-stiffed structures. The design region is established with a 10% margin.

The constraints are imposed on the first two natural frequencies of the system:

$$\begin{cases} g_{\omega 1m} = 1.0 - \dfrac{\omega_1}{\omega_{1P}} \le 0 \\ g_{\omega 1M} = \dfrac{\omega_1}{\omega_{3P}} - 1.0 \le 0 \end{cases} \tag{28}$$

$$\begin{cases} g_{\omega 2m} = 1.0 - \dfrac{\omega_2}{\omega_{1P}} \le 0 \\ g_{\omega 2M} = \dfrac{\omega_2}{\omega_{3P}} - 1.0 \le 0 \end{cases} \tag{29}$$

6.3 Constraint Aggregation for Time-Dependent ULS Constraints

ULS constraints are imposed as stated in [20] and [43]. Requirements are imposed to the strength of the elements of the jacket. The limitations include restrictions on combined axial tension or compression and bending moment (buckling considered) and combined shear, bending moment and torsional moment. Different expressions are defined for submerged and non-submerged elements. For submerged elements actions are combined with hydrostatic pressure and an additional constraint for hoop buckling is imposed. A full description of the expressions and the specific parameters can be found in [52].

The proposed dynamic problem is solved by means of direct integration and thus, the response of the structure is computed at each time-step. This means that the stresses and the constraints are time-dependent. This implies no change in the FLS or the frequency constraints, but the ULS constraints have to be treated differently as different responses of the structure are obtained at each time-step. Dealing with time-dependent constraints is one of the major challenges in structural optimization including a dynamic response.

There are a number of different approaches to manage time-dependent constraints [44–46], for example all the values of the constraints at every single time-step can be used as constraints of the optimization problem (*pointwise constraints approach*). Other approach is to use only the point at which each constraint reaches its maximum value (*worst case approach*). An extensive review of the most used methods is carried out in [17].

Traditional approaches require a high computational effort and show a low efficiency or use non-continuous formulations that are non differentiable and thus produce problems when a sensitivity analysis is required. A number of methods are also non-smooth and can derive in numerical instabilities. The main problem is the fact that they do not accurately represent the actual dynamic state of the structure and there is a loss of information.

In this work, a novel approach to deal with time-dependent constraints in structural dynamics optimization, that is based on constraint aggregation functions, is proposed.

Constraint aggregation is a formulation commonly used in topology optimization for weight minimization under stress constraints. The behavior of the tensional constraints is evaluated over a finite region of the structure by smooth estimating functions to guarantee that they can be used with gradient-based optimization [47, 48]. In this case the Kreisselmeier-Steinhauser aggregation function (KS) is used [49].

The original formulation of the global aggregated function is:

$$KS(g, \rho) = \frac{1}{\rho} \ln \left(\int_\Omega e^{\rho g} d\Omega \right) \tag{30}$$

where g is the value of the constraint being aggregated at each point of the domain, Ω is the domain of aggregation and ρ a parameter of the KS function.

While the selection of Ω for topology optimization allows the aggregation of constraints for specific locations of the domain, it lacks significance in the proposed time-domain aggregation of constraints. Thus, the aggregation is extended over the whole time domain. Particularly, the discrete KS function used is:

$$G_{KS}^j = \frac{1}{\rho} \ln \left(\sum_{i=1}^{N_T} e^{\rho\, g_j(\boldsymbol{x}, t_i)} \right) - \frac{1}{\rho} \ln(N_T) \tag{31}$$

where N_T is the total number of time-steps, $g_j(\boldsymbol{x}, t_i)$ is the value of the j-th constraint at the i-th time-step.

The use of the above formulation for the dynamic optimization problem is able to reduce the large-scale constrained optimization problem while the resulting continuously differentiable global function is suitable for gradient-based optimization and holds information about all the constraints (active or not).

In essence, the KS function contains information about all the constraints and weights them, giving more importance to the most violated or active constraints. The higher the value of ρ, the higher the influence of the violated constraints compared to others. In the limit $\rho \longrightarrow \infty$, the function is equivalent to the *worst case approach*. However it still holds information about other constraints while the worst case approach does not.
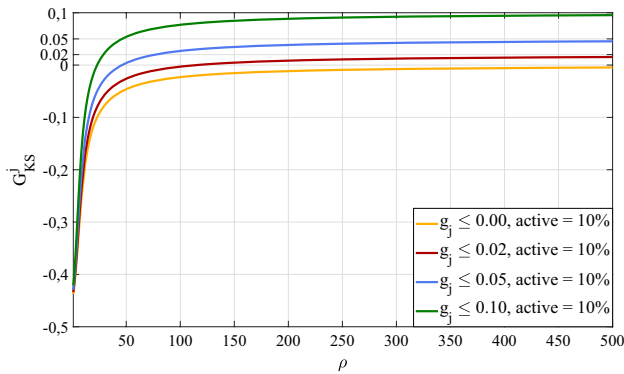
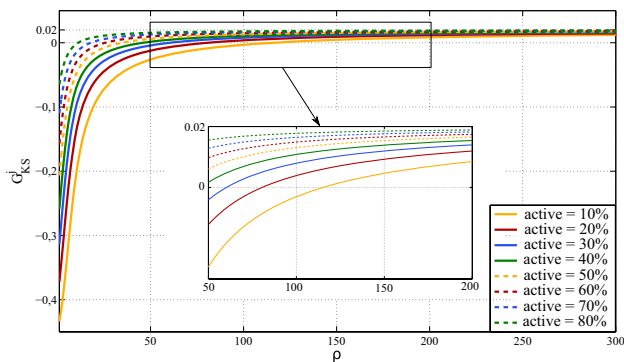**Fig. 11** ρ influence with a 10% of active constraints

Fig. 12 ρ influence allowing a 2% violation of the constraints

Actually, the value of ρ has major influence on the optimized design and the behavior of the aggregated constraint and how accurately it represents the information of all the constraints. In order to select ρ the behavior of G_{KS} was studied. An example model with a number of constraints similar to that of the problem in hands is used. A 10% of the constraints are forced to be violated while the rest remains inactive. Figure 11 shows how the G_{KS} function responds when a certain value for the violation of the constraints is imposed.

As mentioned, the higher the value of ρ the closest the function will be to the maximum value of g_j. For low values of ρ it is also perceived that the KS function does not represent accurately the behavior of the constraints as a 10% of them are violated but the function does not dictate so. A sufficiently large value is needed to detect the violations of the constraints. However, careful must be taken since if ρ is too large, the KS function is excessively nonlinear and produces unstable convergence.

Figure 12 shows that for a large number of violated constraints the requisites for ρ relax since these violated constraints begin to gain importance in the design.

7 Optimization Algorithm and Sensitivity Analysis

7.1 Sequential Linear Programming

The optimization problem proposed is solved by means of Sequential Linear Programming (SLP). Thus, the non-linear optimization problem proposed is solved iteratively by a sequence of approximated linear problems. The design variables $\boldsymbol{x}^*$, that minimize the objective function $F(\boldsymbol{x})$ subject to the constraints $g_j(\boldsymbol{x})$, are obtained modifying the design variables at each iteration by a term $\Delta\boldsymbol{x}$. The linear approximation of the objective function and the constraints is given by:

$$F(\boldsymbol{x}^{k+1}) \approx F(\boldsymbol{x}^k) + \frac{dF(\boldsymbol{x}^k)}{d\boldsymbol{x}}\Delta\boldsymbol{x}^k \tag{32}$$

$$g_j(\boldsymbol{x}^{k+1}) \approx g_j(\boldsymbol{x}^k) + \frac{dg_j(\boldsymbol{x}^k)}{d\boldsymbol{x}}\Delta\boldsymbol{x}^k \tag{33}$$

where $\Delta\boldsymbol{x}^k$ is:

$$\Delta\boldsymbol{x}^k = \theta^k \boldsymbol{s}^k \tag{34}$$

where $\boldsymbol{s}^k$ denotes the direction of modification of the variables and θ^k is the step factor.

Obviously, the direction $\boldsymbol{s}^k$ at each iteration can be obtained by solving the following linear minimization problem:

$$\min\left\{\frac{dF(\boldsymbol{x}^k)}{d\boldsymbol{x}}\Delta\boldsymbol{x}^k\right\}$$
subject to: $\tag{35}$
$$\frac{dg_j(\boldsymbol{x}^k)}{d\boldsymbol{x}}\Delta\boldsymbol{x}^k \le -g_j(\boldsymbol{x}^k) \quad j=1,m$$

Since the linearization of the original problem may trim the feasible design region and also lack accuracy, at each iteration, upper and lower limits are imposed to the maximum variation of the design variables. These are called moving limits and are based on the current values of the variables. These moving limits are stablished as a ±5% of maximum variation of each design variable between iterations. The directions of Eq. (35) are solved by using the Simplex method [50].

7.2 Sensitivity Analysis

The application of Sequential Linear Programming requires a first order sensitivity analysis. Derivatives of the objective function and of the constraints with respect to the design variables have to be computed. Since the constraints depend on the stresses and displacements of the structure, the dynamic equation of motion has to be differentiated to obtain the sensitivities. The sensitivities can be solved

mainly by two methods, Direct Differentiation or Adjoint State Method. The main difference between both methods is in the involved computational cost. Since the number of design variables for the proposed problem is significantly smaller than the number of constraints, Direct Differentiation is clearly advantageous [51].

All the sensitivities, except the fatigue damage sensitivity, are calculated by analitical differentiation. Further details of the particular expressions can be consulted in [52]. The following sections describe the sensitivities that require a special treatment in the differentiation. The sensitivities are expressed in terms of directional derivatives. Given a direction s in which the actual design variables (x) are modified, the derivative for any given function $f(x)$ will be written as:

$$D_s f(x) = \lim_{\theta \to 0} \frac{f(x + \theta s) - f(x)}{\theta} \quad (36)$$

7.2.1 Length Derivative

The structural constraints and the objective function depend on the length of the elements of the jackets. The length is not a design variable but a function of the bottom and top widths of the jacket (geometric design variables). The sensitivity of the length of the elements is explained.

The length of any element can be obtained from the coordinates of its nodes as:

$$L_i = \sqrt{\left(X_{i,2} - X_{i,1}\right)^2 + \left(Y_{i,2} - Y_{i,1}\right)^2 + \left(Z_{i,2} - Z_{i,1}\right)^2} \quad (37)$$

The expression can be differentiated as:

$$
\begin{aligned}
D_s L_i &= \frac{1}{2}\Big(\left(X_{i,2} - X_{i,1}\right)^2 + \left(Y_{i,2} - Y_{i,1}\right)^2 + \left(Z_{i,2} - Z_{i,1}\right)^2\Big)^{-1/2} \\
&\quad \big[2(X_{i,2} - X_{i,1})(D_s X_{i,2} - D_s X_{i,1}) \\
&\quad + 2(Y_{i,2} - Y_{i,1})(D_s Y_{i,2} - D_s Y_{i,1}) \\
&\quad + 2(Z_{i,2} - Z_{i,1})(D_s Z_{i,2} - D_s Z_{i,1})\big] \\
&= \frac{1}{L_i}\big[(X_{i,2} - X_{i,1})(D_s X_{i,2} - D_s X_{i,1}) \\
&\quad + (Y_{i,2} - Y_{i,1})(D_s Y_{i,2} - D_s Y_{i,1}) \\
&\quad + (Z_{i,2} - Z_{i,1})(D_s Z_{i,2} - D_s Z_{i,1})\big]
\end{aligned}
\quad (38)
$$

Thus, the derivatives of the coordinates with respect to the design variables are needed. Figure 13 shows the geometrical changes with a modification of the geometrical variables.

The straight line of the legs of the jacket can be defined by the equation of the X coordinate of the legs at any height Z. Since the origin is set in the center of the jacket then $X(Z) = \mu(Z)/2$ as shown in Fig. 13.

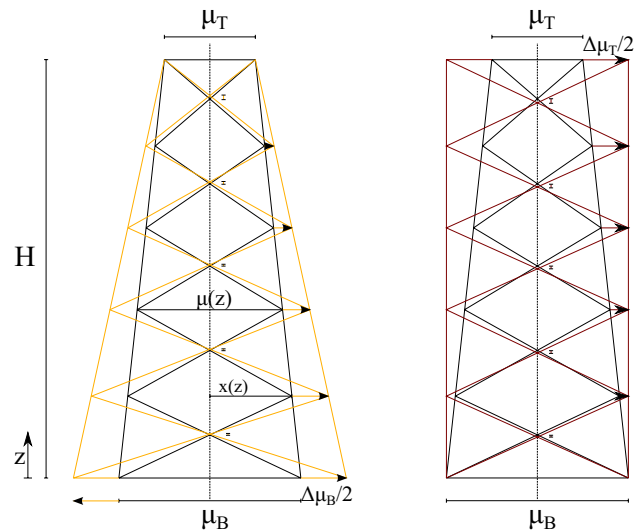$$\mu(Z) = Z\frac{\mu_T - \mu_B}{H} + \mu_B \longrightarrow X(Z) = \frac{Z}{2}\frac{\mu_T - \mu_B}{H} + \frac{\mu_B}{2} \quad (39)$$

Fig. 13 Variation of the coordinates with respect to the geometrical design variables

where μ_B and μ_T are the bottom and top widths of the jacket and H the total height.

The same can be applied to the Y coordinate since the jacket is symmetric in the XY plane:

$$Y(Z) = \frac{Z}{2}\frac{\mu_T - \mu_B}{H} + \frac{\mu_B}{2} \quad (40)$$

The above expressions can be differentiated with respect to the geometrical variables:

$$
\frac{\partial X_i}{\partial \xi} = \begin{cases}
\frac{1}{2}\left(1 - \frac{Z}{H}\right) & \text{if} \quad \xi = \mu_B \\
\frac{1}{2}\frac{Z}{H} & \text{if} \quad \xi = \mu_T \\
0 & \text{otherwise}
\end{cases}
\qquad
\frac{\partial Y_i}{\partial \xi} = \begin{cases}
\frac{1}{2}\left(1 - \frac{Z}{H}\right) & \text{if} \quad \xi = \mu_B \\
\frac{1}{2}\frac{Z}{H} & \text{if} \quad \xi = \mu_T \\
0 & \text{otherwise}
\end{cases}
\quad (41)
$$

The derivative of the Z coordinates is also needed. Since the Z coordinate of the intersection joints of the X braces changes with the design variables, the Z coordinate needs to be expressed as a function of the design variables.

Given any block of the jacket as drawn in Fig. 14, the height of the central node can be expressed in terms of the angle θ, that is:

$$\tan(\theta) = \frac{h_j}{\frac{\mu_{j,1}}{2} + \frac{\mu_{j,2}}{2}} \longrightarrow Z = Z_{j,1} + \tan(\theta)(X - X_0) \quad (42)$$
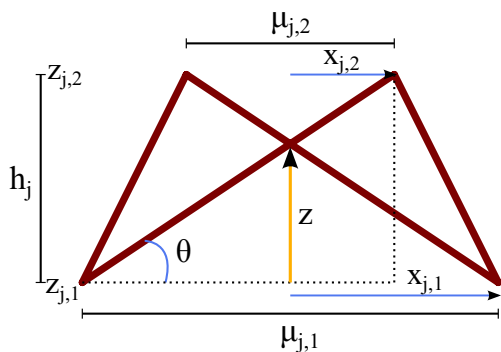
Fig. 14 Z coordinate of the intersection in X joints

where X is the coordinate of the center of the block and $X_0 = -\mu_{k,l}/2$

Then, the local coordinate Z of the joint can be defined as:

$$Z = Z_{j,1} + \frac{h_j\,\mu_{j,1}}{\mu_{j,1} + \mu_{j,2}} \tag{43}$$

Since $\mu_{j,1} = 2X_{j,1}$ and $\mu_{j,2} = 2X_{j,2}$, as shown in Fig. 19:

$$Z = Z_{j,1} + \frac{h_j\,2X_{j,1}}{2X_{j,1} + 2X_{j,2}} \tag{44}$$

These coordinates can be derived with respect to the design variables according to (41). Finally, the derivative of the z coordinate of the intersection nodes can be obtained as:

$$\begin{cases} \dfrac{dZ}{d\mu_B} = \dfrac{\partial Z}{\partial X_{j,1}}\dfrac{dX_{j,1}}{d\mu_B} + \dfrac{\partial Z}{\partial X_{j,2}}\dfrac{dX_{j,2}}{d\mu_B} \\[2mm] \dfrac{dZ}{d\mu_T} = \dfrac{\partial Z}{\partial X_{j,1}}\dfrac{dX_{j,1}}{d\mu_T} + \dfrac{\partial Z}{\partial X_{j,2}}\dfrac{dX_{j,2}}{d\mu_T} \end{cases} \tag{45}$$

where

$$\begin{cases} \dfrac{\partial Z}{\partial X_{j,1}} = \dfrac{h_j(X_{j,1}+X_{j,2}) - h_j X_{j,1}}{(X_{j,1}+X_{j,2})^2} \\[2mm] \dfrac{\partial Z}{\partial X_{j,2}} = -\dfrac{h_j X_{j,1}}{(X_{j,1}+X_{j,2})^2} \end{cases} \tag{46}$$

7.2.2 Aggregated Constraints Derivative

The use of constraint aggregation functions is proposed to aggregate the ULS constraints in the time domain. The methodology allows an enormous reduction of the size of the problem still being differentiable and retaining information about all the constraints, active or not.

The formulation allows to transform a very large set of discrete values of constraints into a continuously differentiable function.

$$D_s G_{KS}^j(\boldsymbol{x}) = \frac{\sum_{i=1}^{N_T} e^{\rho\,g_j(\boldsymbol{x},t_i)} D_s g_j(\boldsymbol{x}, t_i)}{\sum_{i=1}^{N_T} e^{\rho\,g_j(\boldsymbol{x},t_i)}} \tag{47}$$

Note that, even though the constraint aggregation strategy reduces significantly the problem, all the values of the constraints ($g_j(\boldsymbol{x}, t_i)$) and their respective derivatives ($D_s g_j(\boldsymbol{x}, t_i)$) have to be computed at every time-step.

7.2.3 FLS Constraint Derivative

Considering that the number of stress blocks counted by the Rainflow n_i is not affected by changes in the design variables Eq. (24) can be derived to obtain:

$$\begin{aligned} &D_s g_F \\ &= \sum_{l=1}^{N_p} P_l \frac{1}{a} \sum_{i=1}^{k} n_i \left[k'm\frac{1}{t_r}\left(\frac{t}{t_r}\right)^{k'm-1} D_s t(\Delta\sigma_i)^m \right. \\ &\quad \left. + \left(\frac{t}{t_r}\right)^{k'm} m(\Delta\sigma_i)^{m-1} D_s \Delta\sigma_i \right] \end{aligned} \tag{48}$$

The problem of the above expression resides in the calculation of $D_s\Delta\sigma_i$. In [53] authors postulate that an analytical approach to obtain the derivatives of the fatigue life is barely impossible due to the fact that the damage is calculated counting the peaks and valleys of the stresses record. They also stand up for the use of a finite difference scheme to compute the sensitivities.

In [8, 12] the authors propose an analytical formulation to differentiate the stress cycles $\Delta\sigma_i$. The methodology considers the stress cycles individually and not binning them into blocks. The stress ranges $\Delta\sigma_i$ given by the Rainflow are arranged in bins i that arise from various stress cycles of the same amplitude occurring at different times.

Thus, there is not a direct analytical derivative for the stress cycles counted by the rainflow algorithm. Thereby the sensitivity of the damage and so, of the fatigue constraint, need to be assessed differently. In the absence of analytical gradients, finite differences is the common methodology used. However, using a pure finite difference approach involves the modification of every single design variable at least once, solve the simulation, obtain the damage for each perturbation and then find the sensitivities for each variable. This process demands a high computing cost.

Nevertheless, given the analytical derivative of the stresses $\frac{\partial\sigma}{\partial\xi}$ with respect to a design variable ξ, the stresses for a given perturbation of the design variables $\Delta\xi$ can be approximated as:

$$\sigma(\xi + \Delta\xi) \approx \sigma(\xi) + \Delta\xi\frac{\partial\sigma}{\partial\xi} \tag{49}$$

Now the rainflow algorithm can be used on all the perturbed stresses at the hot-spots to obtain the damage of the modified designs $D(\xi + \Delta\xi)$. The numerical derivative of the damage for each design variable can be obtained as:

$$\frac{\partial D}{\partial \xi} \approx \frac{D(\xi + \Delta\xi) - D(\xi)}{\Delta\xi} \tag{50}$$

The above methodology allows to avoid as many solutions of the dynamic equation as design variables are defined. Even though, the cost for this analysis is still extremely high, not only in CPU time but also in storage since the Rainflow algorithm has to be used again to count all the modified stresses.

An additional advantage is that, since the counting process is repeated, the possible variation in the number of cycles n_i, that was neglected by (48), can be accounted for.

Additionally, since the SCF have major impact on the fatigue damage computed, it is mandatory to include their derivatives as part of the sensitivity analysis.

7.2.4 Frequency Constraint Derivative

Constraints are imposed on the first two natural frequencies of the system which are obtained by solving a generalized inverse eigenvalue problem:

$$\boldsymbol{M}\boldsymbol{\phi}_i = \rho_i \boldsymbol{K}\boldsymbol{\phi}_i \tag{51}$$

where ρ_i and $\boldsymbol{\phi}_i$ are the i-th eigenvalue and the corresponding eigenvector respectively.

The sensitivities can be obtained as.

$$
\begin{aligned}
D_s\boldsymbol{M}\boldsymbol{\phi}_i + \boldsymbol{M}D_s\boldsymbol{\phi}_i &= D_s\rho_i \boldsymbol{K}\boldsymbol{\phi}_i + \rho_i D_s\boldsymbol{K}\boldsymbol{\phi}_i + \rho_i \boldsymbol{K}D_s\boldsymbol{\phi}_i \\
D_s\boldsymbol{M}\boldsymbol{\phi}_i + \left(\boldsymbol{M} - \rho_i\boldsymbol{K}\right)D_s\boldsymbol{\phi}_i &= D_s\rho_i \boldsymbol{K}\boldsymbol{\phi}_i + \rho_i D_s\boldsymbol{K}\boldsymbol{\phi}_i \\
&= 0 \\
\boldsymbol{\phi}_i^t D_s\boldsymbol{M}\boldsymbol{\phi}_i + \overbrace{\boldsymbol{\phi}_i^t\left(\boldsymbol{M} - \rho_i\boldsymbol{K}\right)}D_s\boldsymbol{\phi}_i & \\
= \boldsymbol{\phi}_i^t D_s\rho_i \boldsymbol{K}\boldsymbol{\phi}_i &+ \boldsymbol{\phi}_i^t \rho_i D_s\boldsymbol{K}\boldsymbol{\phi}_i
\end{aligned} \tag{52}
$$

since the eigenvectors are $\boldsymbol{K}$-orthogonal:

$$D_s\rho_i \boldsymbol{\phi}_i^t \boldsymbol{K}\boldsymbol{\phi}_i = D_s\rho_i \tag{53}$$

then

$$
\begin{aligned}
\boldsymbol{\phi}_i^t D_s\boldsymbol{M}\boldsymbol{\phi}_i &= D_s\rho_i + \boldsymbol{\phi}_i^t \rho_i D_s\boldsymbol{K}\boldsymbol{\phi}_i \\
D_s\rho_i &= \boldsymbol{\phi}_i^t\left(D_s\boldsymbol{M} - \rho_i D_s\boldsymbol{K}\right)\boldsymbol{\phi}_i
\end{aligned} \tag{54}
$$

8 Numerical Results

This section is intended to show the performance of the optimization method on a coupled OWT model.

8.1 Reference Structure

Even though, the number of offshore wind farms is rapidly increasing and jacket substructures are being installed more and more often, jacket designs are not easily available. One of the most extended public models is the one defined in [54] and completed with the full description of all the elements of the OWT in [27, 55]. Those references detail the geometry and characteristics of the wind turbine tower, the rotor-nacelle assembly, the blades (including aerodynamic properties), transition piece and jacket substructure. Particularly, the defined jacket is the one drawn in Fig. 15. The cross-sections of the elements are displayed in Table 1 and additional properties are shown in Table 2

The tubular structure is a 65.65 m high jacket being its bottom and top widths 12.0 and 8.0 m respectively. The structure is clamped at 50 m deep and formed by 4 levels of X sections and a horizontal bracing bar at the bottom. The S275 steel of the pipes has an elastic modulus $E = 2.1\,10^8\,\text{kN/m}^2$, a poisson modulus of $\nu = 0.3$ and a density of 7.85 t/m. The initial jacket mass is 673.810 t with the proposed model where the references state a mass of 673.718. That means only a 0.014% deviation.

The jacket is formed by 4 different cross-sections, two for the legs, one for the braces and the last one for the 4 vertical bars embedded in the transition piece. This is the initial configuration defined by the UpWind Reference jacket. The optimization design variables are not limited to that classification of the structural elements although they do have to respect the structural symmetry.

8.2 Approximation of Environmental Data

In this numerical example, a test case is presented where a small lumped scatter diagram that comprises the information of a bigger scatter diagram is optimized. Five load cases are imposed where four of them correspond to FLS cases and one for ULS as seen in Table 3. Different rotating speeds are set for each load case according to [55].

In this example 22 design variables are used, 10 diameters, 10 thicknesses and 2 geometry variables distributed according to Fig. 15. A time-step of $\Delta t = 0.1$ was used in the time-integration scheme. With that setup the analysis took nearly 50 min per iteration.

The optimum is reached in 284 iterations and 223 hours of computing time. Optimum design is drawn in Fig. 16 and the evolution of the design and the values of the objective function in Fig. 17. The optimum weight achieved is 302.554 t. The optimum design presents 448 active constraints: 266 ULS, 52 FLS, 128 dimensional and the 2 natural frequency constraints. Table 4 shows the values for the initial and the optimum design variables.
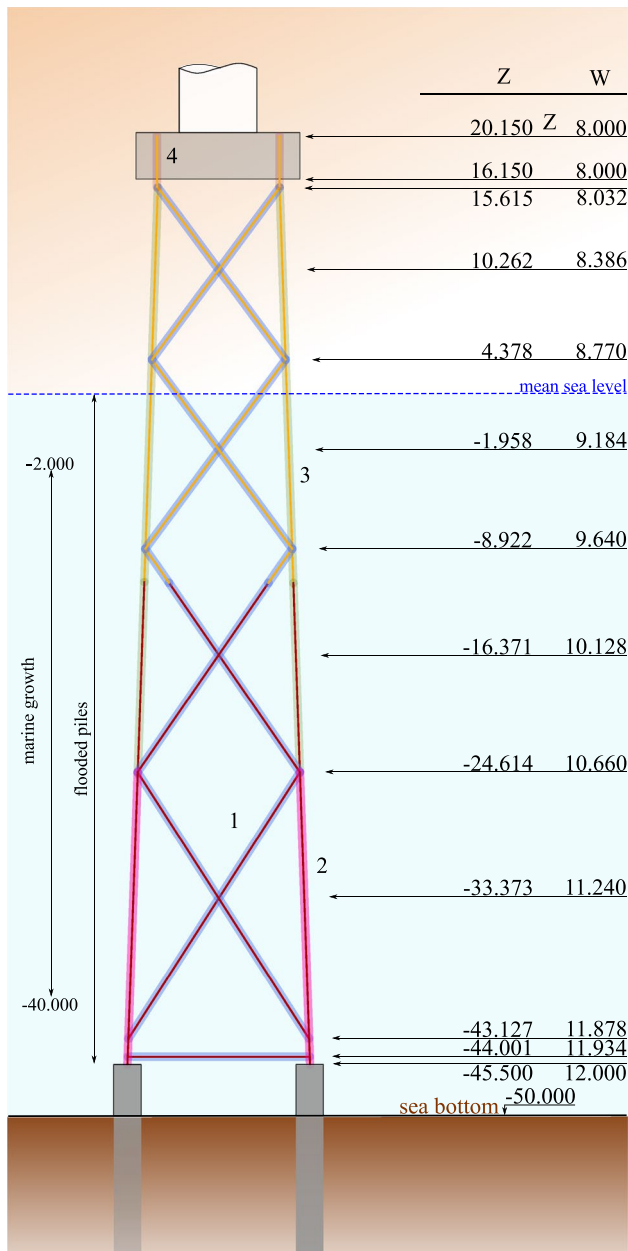
Fig. 15 Jacket geometry

The figure contains the following Z / W label pairs:

Z	W
20.150	8.000
16.150	8.000
15.615	8.032
10.262	8.386
4.378	8.770
-1.958	9.184
-8.922	9.640
-16.371	10.128
-24.614	10.660
-33.373	11.240
-43.127	11.878
-44.001	11.934
-45.500	12.000
-50.000	

mean sea level; -2.000; -40.000; marine growth; flooded piles; sea bottom

Table 1 Cross-sections of the elements of the jacket (see Fig.15)

	D (m)	t (m)	A (m^2)	I (m^4)	J (m^4)
1	0.800	0.020	0.04901	0.00373	0.00187
2	1.200	0.050	0.18064	0.02992	0.01496
3	1.200	0.035	0.12810	0.02175	0.01088
4	1.200	0.040	0.14577	0.00246	0.01227

While 284 iterations might seem too many structural reanalysis, the optimization methodology already reaches a weight of 305.974 t at iteration 78. From that point on, the

Table 2 Additional masses of the model

Additional masses:		
1	Marine growth:	$-40 \le z \le -2$
		$t = 0.100$
		$\rho = 1.1\,\text{t/m}^3$
2	Flooded piles:	$z \le MSL$
		$\rho = 1.025\,\text{t/m}^3$

Table 3 Description of the lumped load cases for ULS and FLS

Case	H_s (m)	T (s)	V_{hub} (m/s)	P (%)
ULS	9.40	13.70	42.73	–
FLS 1	1.07	6.03	2.00	19.163
FLS 2	1.31	5.67	8.00	52.143
FLS 3	2.47	6.71	18.00	22.120
FLS 4	4.46	8.86	30.00	6.574

algorithm oscillates around the optimum. This is caused by the linearization of the constraints and the first order information. The developed methodology could be sped up by the implementation of a second order sensitivity analysis.

The optimum design clearly tends to a wider bottom and top bases. While in the first stage of the optimization process, corresponding to a fast reduction of the objective function, almost every design variable is decreased, from iteration 30 on, most of the variables keep descending while the shape of the jacket starts to increase. That is a consequence of the natural frequency constraints as seen in the following example.

8.3 Impact of the Natural Frequency Constraints

In order to illustrate the high impact the natural frequency constraints have on the optimization process three modified designs are proposed as initial point (Fig. 18).

Designs change in the number of X bracing blocks with the heights of Table 5. Each design is named by the number of X blocks, and their initial weights in order are: 666.04, 673.81, 715.23 and 737.88 tones. Note that all the modified designs keep the mean sea level between two different blocks. Additionally, the 6X jacket is similar to the 5X jacket just dividing the first block into two of the same height. Each block of the structures has its own 4 design variables, separating the section (D, t) of the legs and the section of the braces, except the 6X jacket where the two bottom blocks share the same 4 design variables. The initial distribution of the cross-sections is the same as the previous example. Design variables have been also numbered following the order of Fig. 15.
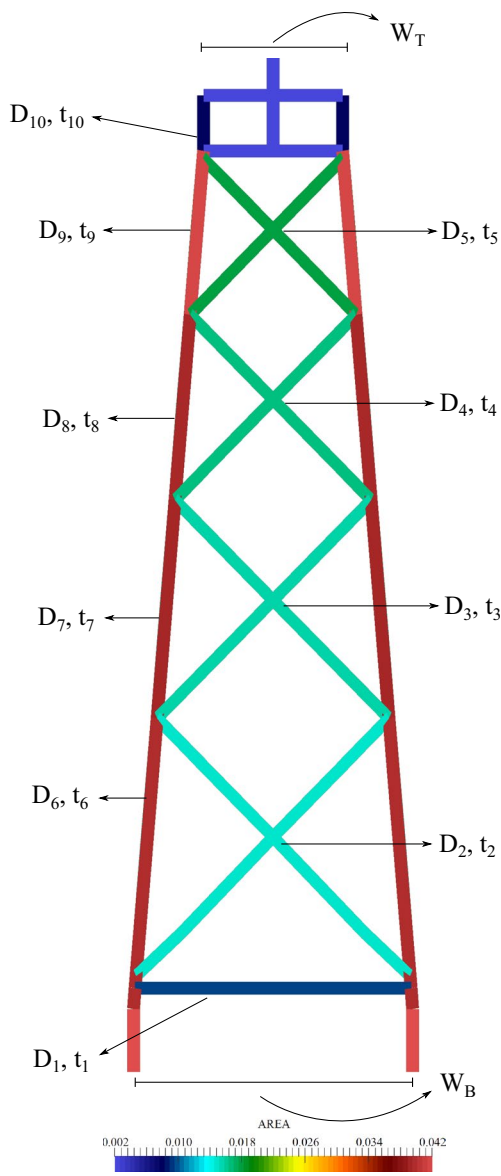
Fig. 16 Optimized design and distribution of the design variables

Structures are subjected to a single load case combining wind and waves. A 6 m high wave with 10 s of period and a shear wind 8 m/s at the hub are applied. The DFF considered is 3 for every joint of the jacket.

Figure 19 plots the value of the objective function through the optimization process for the four designs and also draws their optimum designs. The exact values for the design variables, optimized weight, number of iterations and number of active constraints at the optimum are shown in Tables 6, 7 and 8.

The main perceivable difference between the optimum designs corresponds to the geometrical design variables. The 3X and 5X designs tend to a conical shape where the 4X and the 6X designs are more rectangular shaped. The main

Table 4 Initial and optimum values for the design variables. Diameter in m, thickness in mm, widths in m

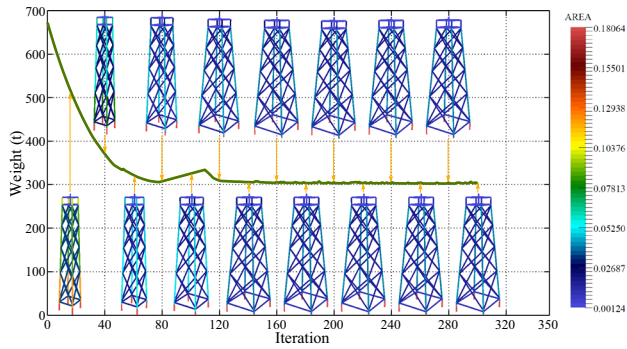|	D_1	D_2	D_3	D_4	D_5	D_6	D_7	D_8	D_9	D_{10}
Initial	0.800	0.800	0.800	0.800	0.800	1.200	1.200	1.200	1.200	1.200
Optimum	0.500	0.500	0.500	0.500	0.500	0.644	0.819	0.619	0.500	0.500
	t_1	t_2	t_3	t_4	t_5	t_6	t_7	t_8	t_9	t_{10}
Initial	20.000	20.000	20.000	20.000	20.000	50.000	35.000	35.000	35.000	40.000
Optimum	5.961	9.411	9.974	10.557	11.494	20.185	15.508	20.878	27.936	4.911
	W_B		W_T							
Initial	12.000		8.000							
Optimum	20.000		9.967							

Fig. 17 Evolution of the objective function and designs
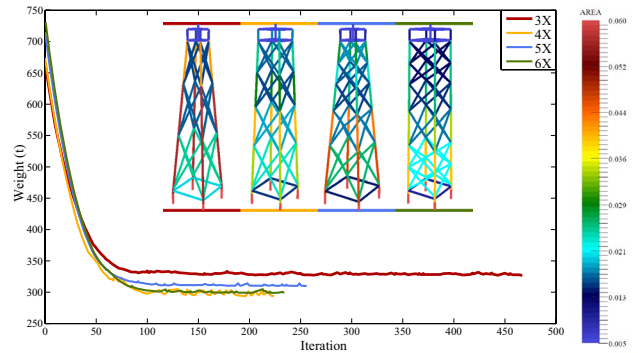

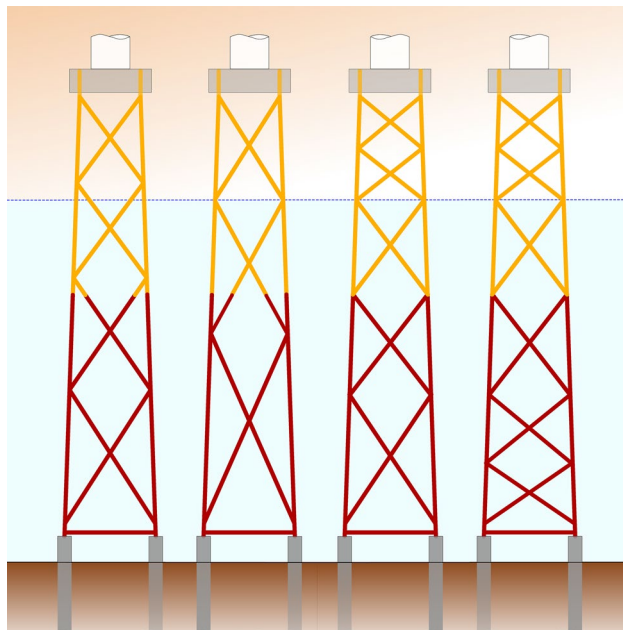**Fig. 19** Evolution of the objective function for the modified designs

Fig. 18 Evolution of the objective function and designs

Table 6 Weight (t), iterations, active constraints and shape design variables (m) at the optimum changing the height of the blocks

	W_{op}	Itera	Active	W_b	W_t
3X	327.165	263	170	14.778	5.663
4X	293.380	196	205	13.862	9.153
5X	309.708	250	304	16.416	6.679
6X	298.874	221	282	12.948	10.967

lowered. Precisely at the point where the first modes reach the lower limit, the algorithm can not keep decreasing all the design variables without violating the constraints. Thereby, the design chooses to increase the geometry design variables and with them the general size of the jacket while it keeps decreasing the sizes of the individual elements. There are two main reasons for this tendency. The first is the fact that the first natural frequencies correspond to global bending modes of vibration and thus, when the size of the bottom and top bases is increased the global inertia of the jacket is raised and helps maintaining the value of the natural frequency. And second, the objective function of the optimization problem is more sensitive to changes in the cross-sections of the elements than in the geometry of the jacket, thereby, to keep reducing the diameters and thicknesses allows a greater reduction of the weight of the structure.

reason for this tendency in the optimum designs is the lower limit for the natural frequency constraints Fig. 20.

As the sizing and geometry design variables initially decrease, so do the stiffness and mass of the structure. Since the reduction is more pronounced in stiffness than in mass, the frequency of the first natural modes of vibration is

Table 5 Height of the X bracing blocks in the modified designs. Dimensions in m

	H_1	H_2	H_3	H_4	H_5	H_6
3x	22.892	20.235	15.615	–	–	–
4x	18.513	15.692	13.300	11.237	–	–
5x	18.701	13.978	10.448	7.809	7.806	–
6x	9.351	9.351	13.978	10.448	7.809	7.806

Table 7 Diameter in meters of the designs changing the height of the blocks

	3X	4X	5X	6X
D_1	0.725	0.500	0.607	0.500
D_2	0.500	0.500	0.500	0.500
D_3	0.500	0.500	0.500	0.500
D_4	0.500	0.500	0.500	0.500
D_5	0.866	0.500	0.500	0.500
D_6	1.084	0.500	0.500	0.500
D_7	0.901	0.778	0.645	0.547
D_8	0.500	0.616	0.822	0.583
D_9	–	0.563	0.615	0.612
D_{10}	–	0.500	0.673	0.501
D_{11}	–	–	0.530	0.544
D_{12}	–	–	0.500	0.500

Table 8 Thickness in millimeters of the designs changing the height of the blocks

	3X	4X	5X	6X
t_1	8.6	9.4	7.2	5.9
t_2	15.8	15.0	16.6	13.4
t_3	10.3	11.7	10.8	10.8
t_4	9.8	9.9	9.7	9.4
t_5	21.2	10.3	10.1	8.0
t_6	16.9	22.5	11.3	8.2
t_7	14.9	16.6	23.7	23.9
t_8	4.1	15.2	17.1	19.2
t_9	–	14.1	13.0	13.3
t_{10}	–	11.0	10.7	16.2
t_{11}	–	–	16.9	14.3
t_{12}	–	–	5.4	6.5

9 Conclusions

In this work a methodology for the optimization of steel jackets for offshore wind turbines is proposed. The whole system behavior is simulated by means of a fully-coupled model (including the substructure, the transition piece, the turbine tower, the rotor-nacelle assembly and the blades).

The computational model takes into account the continuous rotation of the blades. The dynamics of the structure are solved by means of a non-linear time-integration algorithm. A new method is proposed for assessing the long-term fatigue damage of the steel joints on the basis of a linear extrapolation of the results predicted by short-term simulations. A novel formulation for the treatment of time-dependent constraints in transient response optimization of structures is proposed. This technique is based on constraint
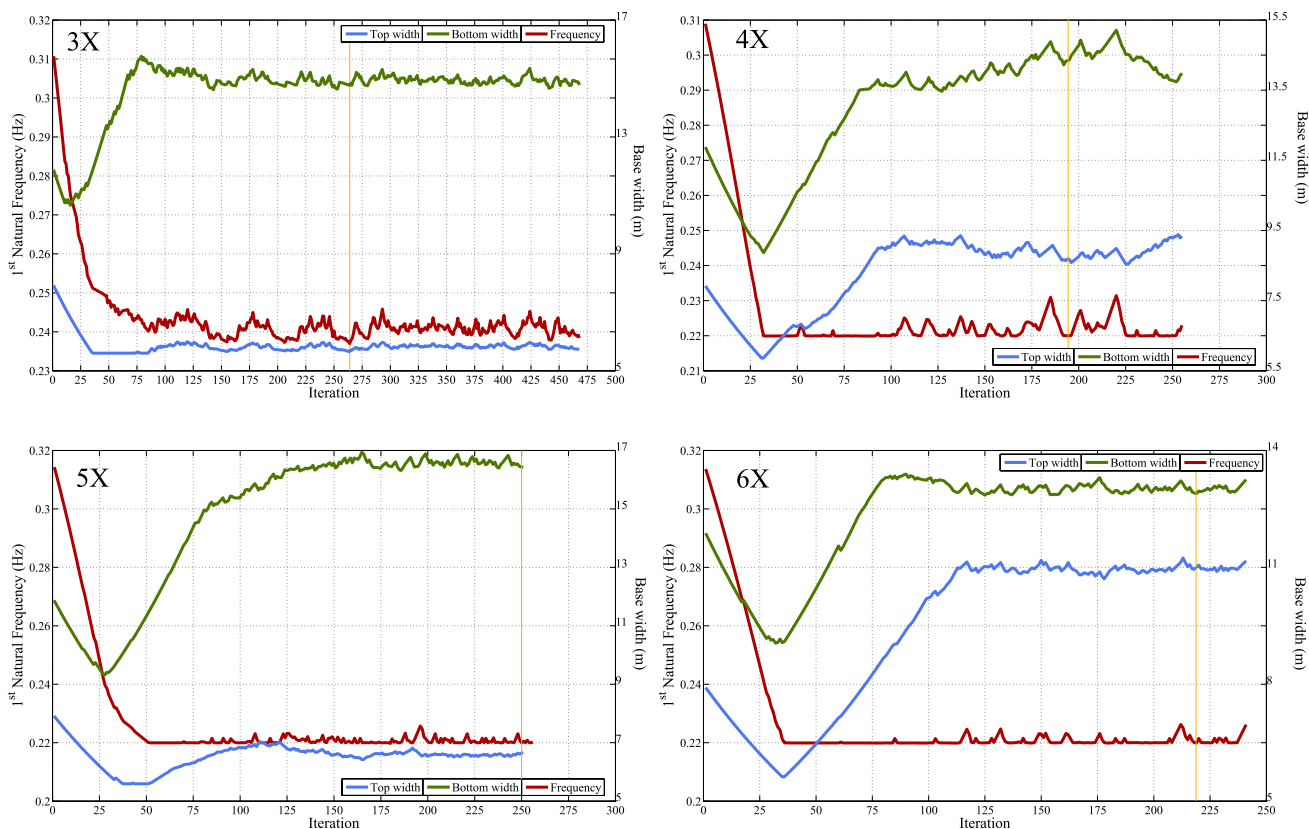

Fig. 20 Evolution of the objective function and designs

aggregation functions, and it allows to perform an efficient and condensed treatment of the time-dependent constraints in this kind of structural dynamics problems without loss of information on the structural response. Constraints that account for restrictions on the fatigue damage and on natural frequencies are also imposed. The objective function to be minimized is the weight of the jacket. The design variables are two parameters that define the general shape of the jacket, along with the dimensions of the cross-sections of the structural members, thus giving a mixed (shape and sizing) optimization model. The optimization algorithm is based on the Sequential Linear Programming concept. The proposed methodology has been tested in real problems. The results exhibit significant weight reductions, and prove the efficiency, the reliability and the robustness of the proposed techniques. It can be noticed that the natural frequency constraints seem to have the most determinant impact on the optimum shape of the structure. From the reverse point of view, taking into account the variables that define the shape of the jacket in the optimization process allows for significant further reductions in the weight of the structure without violating the natural frequency constraints.

Compliance with Ethical Standards

Conflict of interest The authors declare that they have no conflict of interest.

Research Involving Human and Animal Participants The research does not involve neither human participants nor animals

Informed Consent All the authors are informed and provided their consent.

References

1. Chakrabarti S (2005) Handbook of offshore engineering, vol 1. Elsevier, Amsterdam
2. Yoshida S (2006) Wind turbine tower optimization method using a genetic algorithm. Wind Energy 30:453–470
3. Karadeniz H, Togan V, Daloglu A, Vrouwenvelder T (2010) Reliability-based optimisation of offshore jacket-type structures with an integrated-algorithms system. Ships Offshore Struct 5:67–74
4. Yan Q, Zhang Z, Cui L, Wang Y (2010) Structural optimization of offshore jacket platform based on ansys. Adv Mater Res 163–167:3029–3033
5. King J, Cordle A, McCann G (2013)Cost reductions in offshore wind turbine jacket design using integrated analysis and advanced control. In: Proceedings of the twenty-third international offshore and polar engineering, Anchorage Alaska, USA
6. Nasseri T, Shabakhty N, Afshar MH (2014) Study of fixed jacket offshore platform in the optimization design process under environmental loads. Int J Marit Technol 2:75–84
7. Zwick D, Muskulus M, Moe G (2012) Iterative optimization approach for the design of full-height lattice towers for offshore wind turbines. Energy Procedia 24:297–304
8. Chew KH, Muskulus M, Zwick D, Ng E, Tai K (2013) Structural optimization and parametric study of offshore wind turbine jacket structure. In: Proceedings of the twenty-third international offshore and polar engineering, Anchorage Alaska, USA
9. Muskulus M, Schafhirt S (2014) Design optimization of wind turbine support structure: a review. J Ocean Wind Energy 1:12–22
10. Schafhirt S, Zwick D, Muskulus M (2014) Reanalysis of jacket support structure for computer-aided optimization of offshore wind turbines with a genetic algorithm. J Ocean Wind Energy 1:209–216
11. Schafhirt S, Zwick D, Muskulus M (2016) Two-stage local optimization of lattice type support structures for offshore wind turbines. Ocean Eng 117:163–173
12. Chew KH, Tai K, Ng E, Muskulus M (2016) Analytical gradient-based optimization of offshore wind turbine substructures under fatigue and extreme loads. Marine Struct 47:34–41
13. Oest J, Sorensen R, Overgaard LCT, Lund E (2017) Structural optimization with fatigue and ultimate limit constraints of jacket structures for large offshore wind turbines. Struct Multidiscipl Optim 55:779–793
14. Sandal K, Latini C, Znia V, Stolpe M (2018) Integrated optimal design of jackets and foundations. Marine Struct 61:398–418
15. Hasselbach P, Natarajan A, Jiwinangun RG, Branner K (2013) Comparison of coupled and uncoupled load simulations on a jacket support structure. In: 10th deep sea offshore wind R&D conference, DeepWind'2013, Trondheim Norway
16. Hansen MOL (2008) Aerodynamics of wind turbines, 2nd edn. Earthscan, London
17. Kang BS, Park GJ, Arora JS (2006) A review of optimization of structures subjected to transient loads. Struct Multidiscipl Optim 31:81–95
18. Passon P, Branner K (2014) Load calculation methods for offshore wind turbine foundations. Ships Offshore Struct 9:433–499
19. Yeter B, Garbtov Y, Soares CG (2015) Fatigue damage assessment of fixed offshore wind turbine tripod support structures. Eng Struct 101:518–528
20. DNV-OS-C101 (2014) Design of offshore steel structures, general (LRFD Method). Det Norske Veritas
21. BS-EN-ISO-19902:2007+A1 (2013) Petroleum and natural gas industries - Fixed steel Offshore structures. British Standard
22. Burton T, Sharpe D, Jenkins N, Bossany E (2001) Wind energy handbook. Wiley, Chichester
23. Hau E (2006) Wind turbines. fundamentals, technologies, application, economics. Springer, Berlin
24. Manolas D, Riziotis V, Voutsinas S (2015) Assessing the importance of geometric nonlinear effects in the prediction of wind turbine blade loads. J Comput Nonlinear Dyn 10:1–15
25. Dolan DS, Lehn PW (2006) Simulation model of wind turbine 3p torque oscillations due to wind shear and tower shadow. IEEE Trans Energy Convers 21:717–723
26. Morison J, O'Brien M, Johnson J, Schaaf S (1950) The force exerted by surface waves on piles. Pet Trans 189:149–154
27. Vorpahl G, Popko W, Kaufer D (2012) Description of a basic model of the UpWind reference jacket for code comparison in the OC4 project under IEA Wind Annex XXX. Tech. Report. Fraunhofer Institute for Wind Energy and Energy System Technology

28. DNV-OS-J101 (2010) Design of offshore wind turbine structures. Det Norske Veritas

29. Hughes TJ (1987) The finite element method. Linear static and dynamic finite element analysis. Prentice-Hall Inc, New Jersey

30. Chang SY (2004) Studies of Newmark method for solving non-linear systems: I basic analysis. J Chin Inst Eng 27:651–662

31. DNV-RP-C203 (2011) Fatigue design of offshore steel structures. Det Norske Veritas

32. Palmgren A (1924) Die lebensdauer von kugellagern. VDI-Zeitschrift 68:339–341

33. Efthymiou M (1988) Development of scf formulae and general-ised influence functions for use in fatigue analysis. In: Offshore tubular joints conference on recent developments in tubular joints technolgy. London

34. Endo T, Matsuishi M, Mitsunaga K, Kobayashi K, Takahashi K (1974) Rain flow method—the proposal and the applications. Memoir Kyushu Institute Technical Engineering

35. ASTM-E1049-85(2011)e1 (2011) Standard practice for cycle counting in fatigue analysis. American Society for Testing and Materials

36. Dirlik T (1985) Applications of computers in fatigue analysis. PhD thesis. University of Warnick

37. Ragan P, Manuel L (2007) Comparing estimates of wind turbine fatigue loads using time-domain and spectral methods. Wind Eng 31:83–89

38. Mohammadi SF, Galgoul NS, Starossek U, Videiro PM (2016) An efficient time domain fatigue analysis and its comparison to spectral fatigue assessment for an offshore jacket structure. Marine Struct 49:97–115

39. Jia J (2014) Investigations of a practical wind-induced fatigue calculation based on nonlinear time domain dynamic analysis and a full wind-directional scatter diagram. Ships Offshore Struct 9:272–296

40. Kvittem MI, Moan T (2015) Time domain analysis procedures for fatigue assessment of a semi-submersible wind turbine. Marine Struct 40:38–59

41. Stieng LES, Hetland R, Schafhirt S, Muskulus M (2015) Rela-tive assessment of fatigue loads for offshore wind turbine sup-port structures. In: 12th deep sea offshore wind R&D conference. Norway

42. Martens JH (2014) Topology optimization of a jacket for an off-shore wind turbine. PhD thesis. Norwegian University of Science and Technology

43. Norsok (2004) Design of steel structures. Standards Norway

44. Wang Q, Arora JS (2005) Alternative formulations for transient dynamic response optimization. Am Inst Aeronaut Astronaut J 43:2188–2195

45. Wang Q, Arora JS (2009) Several simultaneous formulations for transient dynamic response optimization: an evaluation. Int J Numer Methods Eng 80:631–650

46. Hsieh C, Arora JS (1984) Design sensitivity analysis and optimi-zation of dynamic response. Comput Methods Appl Mech Eng 43:195–219

47. París J, Navarrina F, Colominas I, Casteleiro M (2009) Topology optimization of continuum structures with local and global stress constraints. Struct Multidiscipl Optim 39:419–437

48. Lambe AB, Graeme JK, Martins JR (2017) An evaluation of con-straint aggregation strategies for wing box mass minimization. Struct Multidiscipl Optim 55:257–277

49. Kreisselmeier G, Steinhauser R (1979) Systematic control design by optimizing a vector performance indicator. In: Symposium on computer-aided design of control systems. IFAC Zurich, Switzerland

50. Dantzig GB, Thapa MN (1997) Linear programming I: introduc-tion. Springer, New York

51. Navarrina F, López-Fontán S, Colominas I, Bendito E, Casteleiro M (2000) High order shape design sensitivity: a unified approach. Comput Methods Appl Mech Eng 188:681–696

52. Couceiro I (2018) Structural optimization of steel jackets for off-shore wind turbines considering dynamic response and fatigue constraints. PhD thesis, Universidade da Coruña

53. Choi KK, Kim NH (2005) Structural sensitivity analysis and opti-mization, vol 2. Springer, New York

54. de Vries W (2011) Final report WP 4.2: Support structure con-cepts for deep water sites: deliverable D4.2.8. Technical Report. UpWind Project

55. Jonkman J, Butterfield S, Musial W, Scott G (2009) Definition of a 5-MW reference wind turbine for offshore system development. Technical report. NREL, National Renewable Energy Laboratory